https://doi.org/10.14233/ajchem.2025.33904



Spectral Analysis and Biological Evaluation of 3,5-Dimethyl-1-[2-(1-methyltetrazol-5-yl)-sulfanylacetyl]-2,6-diphenyl-piperidin-4-one: Crystal Structure, Hirshfeld Surface, Antimicrobial Activity and Dipeptidyl Peptidase IV Inhibition

M.V. Muppuli¹, K. Rajesh^{1,*,0}, K. Anandan^{1,0}, P. Devendran^{2,0}, P. Kurinjinathan^{3,0} and A. Mani^{4,0}

Received: 21 April 2025;

Accepted: 9 June 2025;

Published online: 30 June 2025;

AJC-22043

A single crystal of 3,5-dimethyl-1-[2-(1-methyltetrazol-5-yl)sulfanylacetyl]-2,6-diphenyl-piperidin-4-one (DMTSDPO) has been synthesized and extensively characterized using analytical techniques, which involves 1H NMR, infrared, mass spectroscopy and single crystal X-ray diffraction (SXRD). DMTSDPO is a triclinic crystal system with $P\bar{1}$ space group, with cell dimensions a = 13.301(3) Å; b = 17.687(4) Å; c = 20.615(4) Å and α = 89.928(10)°; β = 89.760(11)°; γ = 72.648(10)°, V= 4628.7(16) and Z= 8. The molecular structure was identified through conservative method and refined with SHELXL-97, which produced a final R-value of 0.0446. The Hirshfeld surface evaluation has been employed to determine the power of interactions involving hydrogen bonds between molecular pairs, revealing predominant contributions from H···H and N···H intermolecular contacts. The derivatives were subjected to *in vitro* antimicrobial assays against bacterial and fungal strains, with DMTSDPO exhibiting significant activity against *E. coli*. The elusive mechanism of action for piperidine derivatives prompted a molecular docking study, shedding light on the active site region, binding modes and interactions of active site residues with dipeptidyl peptidase IV (DPP4). This investigation contributes to a detailed understanding of the compounds mechanism of action and holds promise for the design of novel, potent drug molecules.

Keywords: Density functional theory, Hirshfeld surface evaluation, Molecular docking, Dipeptidyl, Single crystals.

INTRODUCTION

Nitrogen-containing heterocycle molecules, particularly piperidin-4-ones compounds, have gained importance due to their miscellaneous biological characteristics, which include antiviral, insecticidal, antitumor [1], analgesic, fungicidal [2], local anaesthetic, anticancer [3,4], anti-inflammatory, antimicrobial, bactericidal, herbicidal, antihistaminic, CNS stimulant and depressant activities [5-7]. Compounds with an amide bond linkage have exhibit an extensive variety of biological activities, which includes antibacterial activities [8], anti-inflammatory [9], antimalarial and general anesthetics [10]. Antihistaminic medicines, narcotic analgesics, tranquilizers and hypotensive drugs all include a piperidine ring [11]. Various piperidine derivatives refer as the skeletons for a variety of

alkaloids [12]. The piperidone heterocycle primarily exists in chair conformity [13,14], but depending on the replacement, its arrangement and conformation may change [15,16].

Piperidones also perform an essential part in medicine since they are necessary chiral intermediary substances in the synthesis of a wide range of synthetic, natural and semi-synthetic pharmacological agents with effective cancer prevention and anti-HIV characteristics [17]. *Trans*-platinum piperidine compounds should be evaluated for effectiveness in tumor-bearing animals [18]. Nitrogen heterocycles with diphenylacetyl substituents show antihypertensive action [19-22]. The synthesis of 4-piperidones is currently being studied because of its potential therapeutic applications [23,24]. Similar to other alkaloids, like 4-peridones were found to lower blood cholesterol levels [25,26]. Aridoss *et al.* [27-31] studied the antibacterial, anal-

This is an open access journal, and articles are distributed under the terms of the Attribution 4.0 International (CC BY 4.0) License. This license lets others distribute, remix, tweak, and build upon your work, even commercially, as long as they credit the author for the original creation. You must give appropriate credit, provide a link to the license, and indicate if changes were made.

Department of Physics, Centre for Hydrogen Energy Research (HER), Academy of Maritime Education and Training, Kanathur-603112, India

²Department of Physics, Dayananda Sagar Academy of Technology and Management, Bangalore-560082, India

³Department of Physics, PSG College of Arts and Science, Coimbatore-641014, India

⁴Department of Physics, Muthayammal Engineering College (Autonomous), Rasipuram-637408, India

^{*}Corresponding author: E-mail: krishjayarajesh@gmail.com

gesic and chloroacetyl and heterocyclic acetyl derivatives of 2,6-diarylpiperidin-4-ones demonstrate antipyretic effects, as well as alterations in the piperidone ring conformation.

2,6-Dimethylnicotinamide N-oxide moiety is the most suitable option on the proper side [32,33]. The piperidine sub structure was a common fundamental feature observed in many alkaloids [33], natural compounds and therapeutic prospects [34]. The piperidine ring is an essential chemical component in both natural as well as therapeutically active drugs. Piperidine compounds have several biological activities, including analgesics antihypersensitive, nervous system depression, antiviral in nature and bactericidal actions [35-37]. These have raised significant awareness due to their structure, reactivity, synthesis and biological properties. Crystallographic investigations of piperidine derivatives have been conducted in order to determine their molecular conformation and other essential features. In this study, the synthesis, spectral characterization and biological evaluation of 3,5-dimethyl-1-[2-(1-methyl-tetrazol-5-yl)sulfanylacetyl]-2,6-diphenyl-piperidin-4-one was carried out. In addtion, the molecular docking, molecular modelling, Hirshfeld surface evaluation and DFT computational simulations on the B3LYP/6-311G (d,p) functional basis set were also carried out.

EXPERIMENTAL

Synthesis of 3,5-dimethyl-1-[2-(1-methyltetrazol-5-yl)sulfanylacetyl]-2,6-diphenyl-piperidin-4-one (DMTSDPO): To a 10 mL of anhydrous DMF, N-chloroacetyl-3,5-dimethyl-2,6-diphenylpiperidin-4-one (2.0 g) and 5-mercapto-(1-methyl tetrazole) (0.58 g) were added, then followed by the addition of K₂CO₃ (1.03 g). The reaction mass was magnetic stirred for 1 h at room temperature followed by heating to 50 °C and stirred. Following the accomplishment of the reaction, the mixture was quenched in water, the resulting substance was retrieved with dichloromethane and the resulting layer became concentrated according to vacuum. Ethanol was added to the residue as well as stirred instantaneously at 0 to 5 °C. The resulting solid was filtered, washed with cold ethanol, as well as dried out at 60 °C. Initial attempts were made to conduct the reaction using an organic base like triethylamine and solvents like toluene or dichloromethane, but the reaction took more time and some percentage of starting material remains even after several hours hence DMF and K₂CO₃ was chosen as solvent and base, respectively where the reaction completed within 1-2 h at 60 °C. Yield: 85% and m.p.: 151 °C.

Characterization: FT-IR (model: Perkin Elmer FT-IR 8000 spectrophotometer) spectrum analysis was performed on the crystal utilizing the KBr pellet technique in the 4000-400 cm⁻¹ region. Utilizing TMS as an internal standard, ¹H and ¹³C NMR spectra were captured using a Bruker AV III 500 MHz spectrometer. Waters Micromass Q-Tof Micro Mass Spectrometers using electrospray ionization (ESI) and atmospheric pressure chemical ionization (APcI) sources recorded mass spectra from 4000 amu in quadruple and 20000 amu in ToF.

Single crystal X-ray diffraction (SXRD): X-ray diffraction data has been gathered by employing a Bruker axs Kappa APEXII CCD diffractometer as well as graphite-monochromatized $MoK\alpha$ radiation ($\lambda = 0.71073 \text{ Å}$). The results were exami-

ned using the A SAINT software package [38], the framework was resolved and refined utilizing simple techniques and F2 was determined via a full-matrix the least-squares approach in the SHELXL-97 package [39,40]. The molecular visualizations were developed through PLATON [41] and ORTEP-3 [42]. The hydrogen atoms were set up computationally and permitted to ride on their parental atoms of C, with the C-H separation repaired among 0.93-0.97 Å. The parent atom's relocation variables were restricted to 1.2 Ueq.

Hirshfeld surface analysis (HS): Surface evaluation [43] for the molecule was used to visualize the intermolecular interactions and associated with two-dimensional fingerprint plots [44] were generated with the CrystalExplorer [45] software.

Molecular docking: The crystalline arrangement of DPP4 receptor molecules (PDB ID: 2OQI) was obtained from RCSB (PDB) [46]. Molecular modelling simulations occurred using the Schrödinger suite's Induced Fit Docking module. The best-docked structure/pose was selected according to upon three criteria: the Glidescore (Gscore) function, glide energies and the total amount of residuals matches (hydrogen bonds) with the unique drug multifaceted. All the computing effort was executed employing several modules from Schrödinger Suite 2011 software [47] and a Red Hat Enterprise Linux version 5.0 association operating on the Pentium D computer.

Test microorganisms: The organisms *viz*. Gram-negative bacteria *Pseudomonas aeruginosa* (ATCC-1934) and *Escherichia coli* (ATCC-2939); Gram-positive bacteria *Staphylococcus aureus* (ATCC-2940) and fungal strain of *Candida albicans* (ATCC 10231) were obtained from ATCC, Pune, India. The isolates were stored in brain heart infusion (BHI) broth with 50% glycerol at -70 °C.

Antimicrobial assay: The antimicrobial character-istics of the compound against various pathogens were tested on nutritional broth using micro broth dilution [48]. Compound was dissolved in DMSO at 1 mg/mL and dispersed at different concentration (20, 40, 60, 80 and 100 μ g/mL). To inoculate a 96-well polystyrene microplate with 180 μ L suspensions of mid-log microorganisms in nutrient broth, aliquots (20 μ L) of each dilution were distributed. The negative control was 100% DMSO, whereas the positive control was the pathogen alone, free of any chemicals. Microplates were subjected to incubation at 37 °C and examined optically after 24 h. After 24 h of the incubation process, the absorption at 595 nm was determined employing a microplate reader (Bio-Rad, USA) and the minimal inhibitory concentration (MIC) was estimated by comparing absorption to the development of controls.

RESULTS AND DISCUSSION

Infrared spectral studies: Selected diagnostic bands present in absorption offer significant information about the C-H and carbonyl stretching frequencies of the compound. The IR spectrum reveals a typical band at 1713 cm⁻¹, revealing C=O stretching. In addition, the compound exhibits a strong band at 1611 cm⁻¹ corresponding to the N-C=O group. Furthermore, this is supported by the occurrence of robust bands in the region 3061-2877 cm⁻¹, likely attributed to the C-H fragments (Fig. 1).

¹H NMR spectral studies: The ¹H NMR spectral analysis were obtained at 400 MHz on a Bruker Ultra Shield, with DMSO- d_6 as solvent and TMS as an internal reference. The single selective chemical has been validated using ¹H NMR data. A new doublet band appears at 0.95 ppm (d, J = 6.32 Hz, 6H; 7 and 8-CH₃), owing to the hydrogen atoms of the methyl group. The signals of C-H protons appear as a very broad singlet in the region between 5.55 ppm (bs, 2H; 2 and 6-CH) and 3.12 ppm (bs, 2H; 3 and 5-CH) for the respective compound. Moreover, a sharp singlet at 3.91 ppm (s, 3H; 29-CH₃) is assigned to another methyl group present in this compound. Sulfurcontaining methylene protons appear as very broad singlets at 4.27 ppm (bs, 2H; 22-CH₂). The multiple protons of the aromatic ring moiety were observed as multiplets in the range of 7.16-7.36 ppm (m, 10-20, CH) (Fig. 2). These spectral features collectively provide valuable insights into the structure and composition of the synthesized compound.

Mass spectroscopy studies: In positive-ion mode, the molecular ions are typically found as $[M + H]^+$. It meant for the observed mass includes an additional proton. The ESI- MS analysis of the compound exhibited a prominent peak at m/z 436.1, predominantly assigned to $[M + H]^+$ ions. Therefore, the molecular weight of this compound would be 435.1 amu.

$$M = 436.1 - 1$$

 $M = 435.1$ amu

The presence of the strong peak at m/z 436.1 in the positive ion mode shows the stability of the protonated species in the organic solution (Fig. 3). This finding affirms that the identity of compound is maintained in the solution and the molecular structure remains intact in the sample.

Antimicrobial assay: The present investigation examined the antimicrobial effects of compound DMTSDPO against selected human pathogens. Ampicillin, streptomycin and kanamycin were employed for bacterial strains, while amphotericin B served as the reference compounds for fungal activity. The compound showed possible activity at 20 µg/mL or below, moderate activity between 40 and 80 µg/mL, extremely limited or poor activity at 100 µg/mL and no activity against the pathogens at doses more than 100 µg/mL. Antimicrobial screening data revealed that DMTSDPO exhibited significant inhibitory effects against the tested microorganisms, surpassing the reference compounds. Table-1 demonstrates the MIC values for Gram-negative and Gram-positive bacteria, as well as fungal strains. The novel compound displayed increased or dose-dependent activity, suggesting its potential as a potent bactericidal agent, outperforming the reference compounds.

In the evaluation against *C. albicans*, DMTSDPO compound demonstrated high activity at 100 µg/mL, surpassing the reference drug amphotericin B. Fungal inhibition values are presented in Table-1. The incorporation of this compound into the next generation of novel antimicrobial agents appears promising, especially in fungal strain *C. albicans*, combating P, *aeruginosa*, *E. coli* and *S. aureus*.

The MIC values indicated a diverse range of antimicrobial activity for the novel compound against the tested microorganisms, suggesting its potential as an antimicrobial therapeutic agent. Comparisons with previous studies [49], underscored the efficacy of compound DMTSDPO in contradiction of Grampositive and Gram-negative bacteria, further supporting its potential in drug design. Results from this study provide the valuable inputs for the development of extensive novel comp-

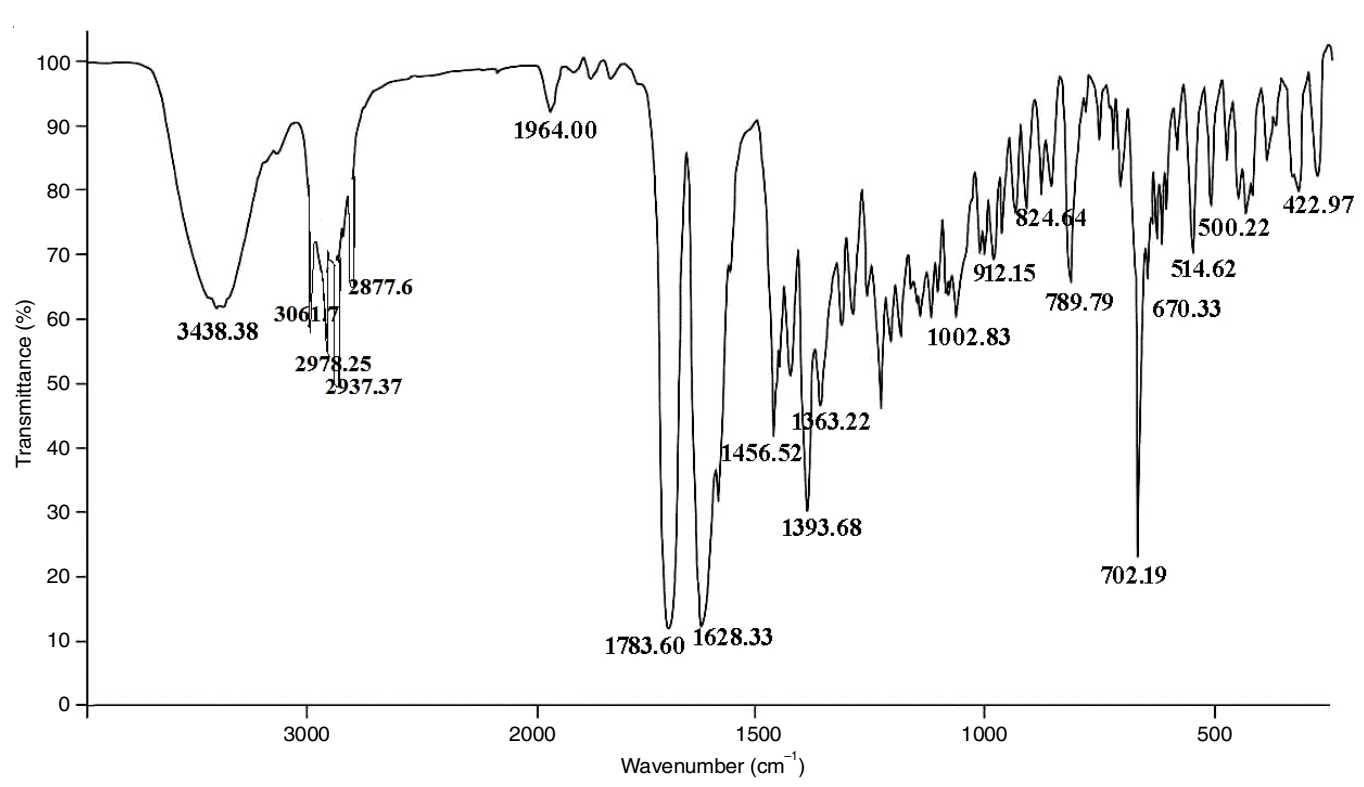


Fig. 1. IR spectrum of DMTSDPO

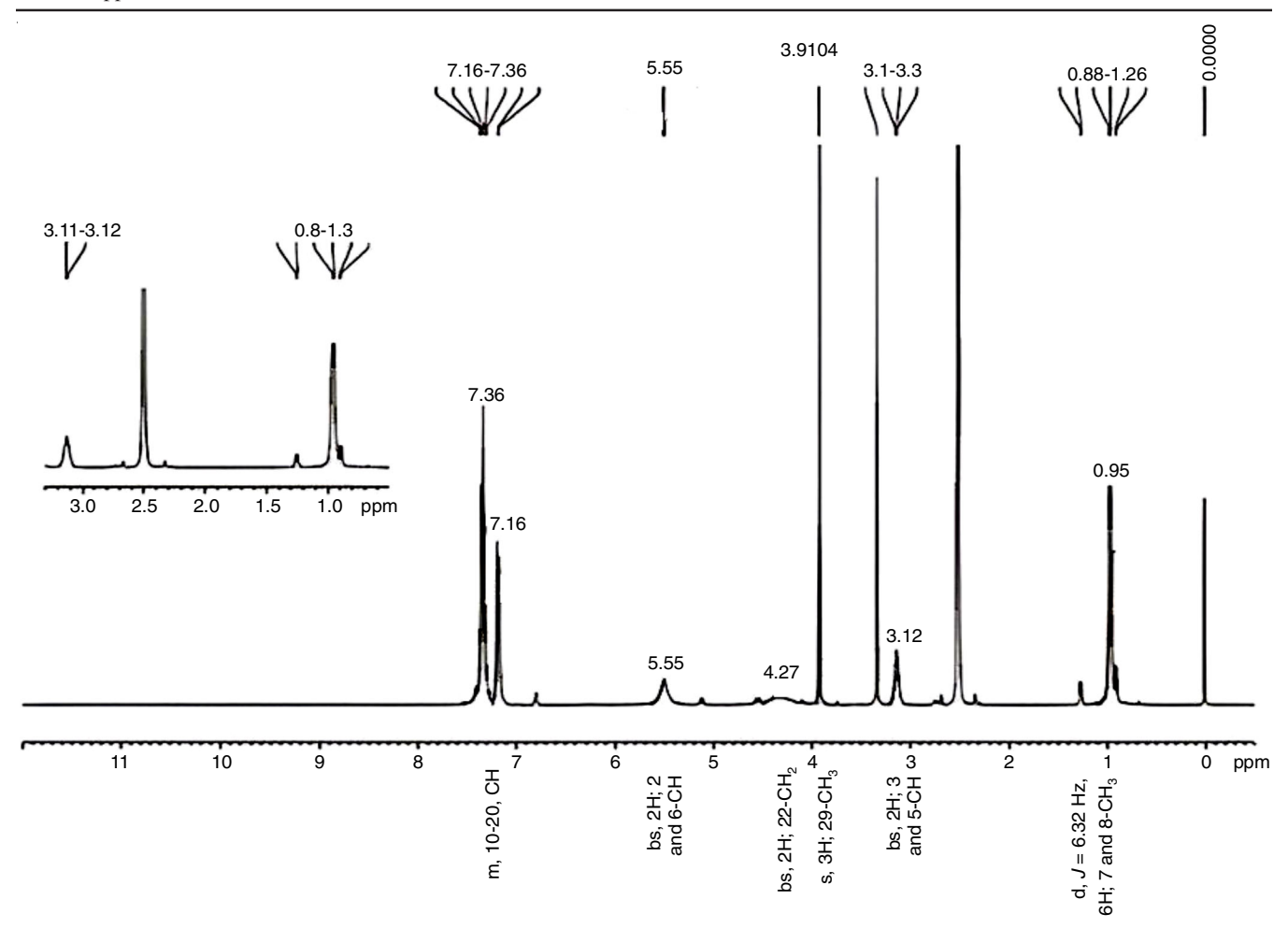


Fig. 2. ¹H NMR spectra of DMTSDPO

TABLE-1 ANTIMICROBIAL ACTIONS OF THE COMPOUNDS AS MIC VALUES ($\mu g/mL$) OF THE SYNTHESIZED COMPOUND				
	Minimum inhibitory concentration (μg/mL)			
Compounds	E. coli ATCC-2939	S. aureus ATCC-2940	P. aeruginosa ATCC-1934	C. albicans ATCC 10231
(1-Methyltetrazol-5-yl) sulfanylacetyl group (1-5)	60	>100	60	100
Ampicillin	20	40	60	-
Streptomycin	50	25	50	-
Kanamycin	40	60	60	-
Amphotericin B	-	-	-	25

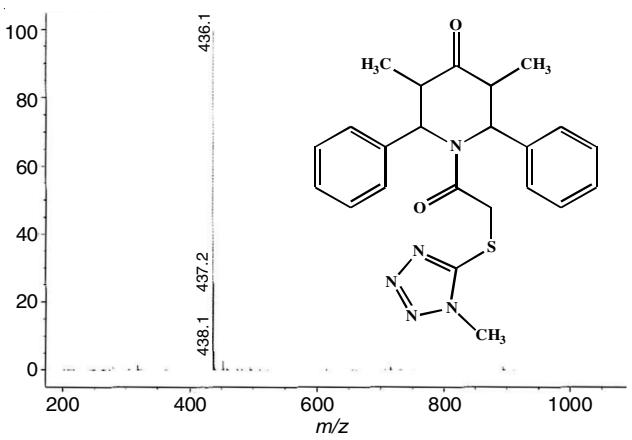


Fig. 3. Mass spectra of DMTSDPO

ounds with the significant antimicrobial contours, similar to standard drugs.

Single-XRD studies: The novel DMTSDPO ($C_{23}H_{25}N_3O_2S$) ccrystallizes in the triclinic crystal system with the $P\overline{1}$ space group. Fig. 4 illustrates the molecular structure of DMTSDPO at a 30% probability level, including atom numbering and displacement ellipsoids [14]. Table-2 incorporates comprehensive details on the X-ray collection of information, framework and organization refinement.

The unit cell of DMTSDPO is composed of four molecules in the asymmetric unit, as illustrated in Fig. 5. These four molecules exhibit considerable similarity and the torsion angles of the substituents on the ring are detailed in Table-3. In each molecule, the piperidine ring adopts a distorted boat configuration,

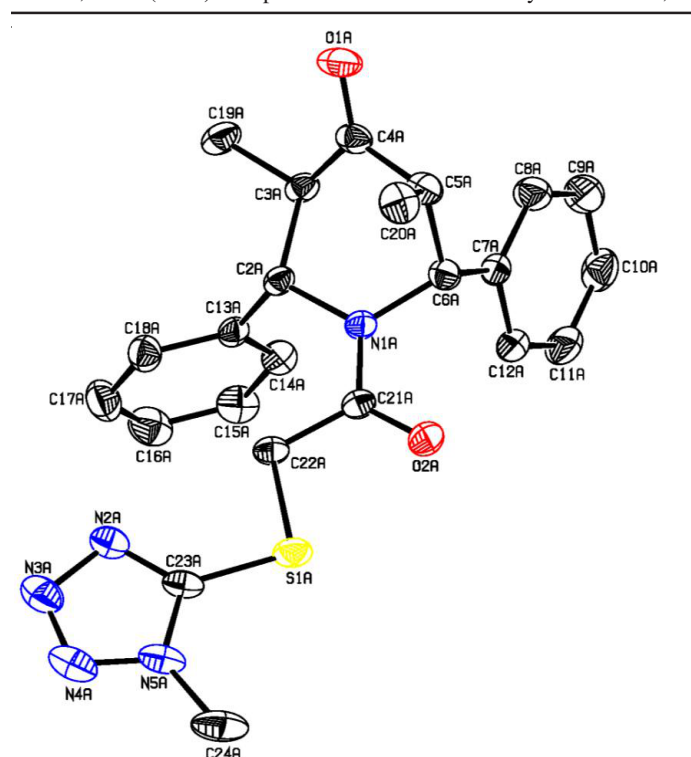


Fig. 4. A vantage point view of the DMTSDPO molecule with the atom labeling system $\,$

TABLE-2 CRYSTAL DATA OF DMTSDPO				
Parameters	Values			
Empirical formula	C ₂₃ H ₂₅ N ₅ O ₂ S			
Molecular weight	435.54			
Temperature in (K)	293(2)			
Wavelength	0.71073			
Space group and crystal system	Pī, Triclinic			
Unit cell dimensions	$a = 13.3007(7) \text{ Å}, \alpha = 89.9280(10)^{\circ}$			
cint cen annonsions	$b = 17.6865(6) \text{ Å}, \beta = 89.760(3)^{\circ}$			
	$c = 20.6147(4) \text{ Å}, \gamma = 72.648(2)^{\circ}$			
Volume (Å ³)	4628.7(3)			
Z, Calculated density	8, 1.250 Mg/m ³			
Absorption coefficient	0.169 mm ⁻¹			
F (000)	1840			
Crystal size	$0.22 \times 0.25 \times 0.28 \text{ mm}$			
Theta range for data collection	0.99 to 26.39°			
Limiting indices	-16<=h<=16, -22<=k<=20,			
<i>e</i>	-25<=l<=25			
Reflections collected/unique	$60189/18611 [R_{int} = 0.0283]$			
Completeness to theta = 26.39	98.00%			
Refinement technique	Full-matrix least-squares on F ²			
Data/parameters/restraints	18611/1129/0			
Goodness of fit on F ²	1.018			
Final R indices [I>2sigma(I)]	R1 = 0.0446, $wR2 = 0.1121$			
R indices (all data)	R1 = 0.0726, $wR2 = 0.1303$			
Largest diff. peak and hole	0.386 and -0.367 e.Å ⁻³			

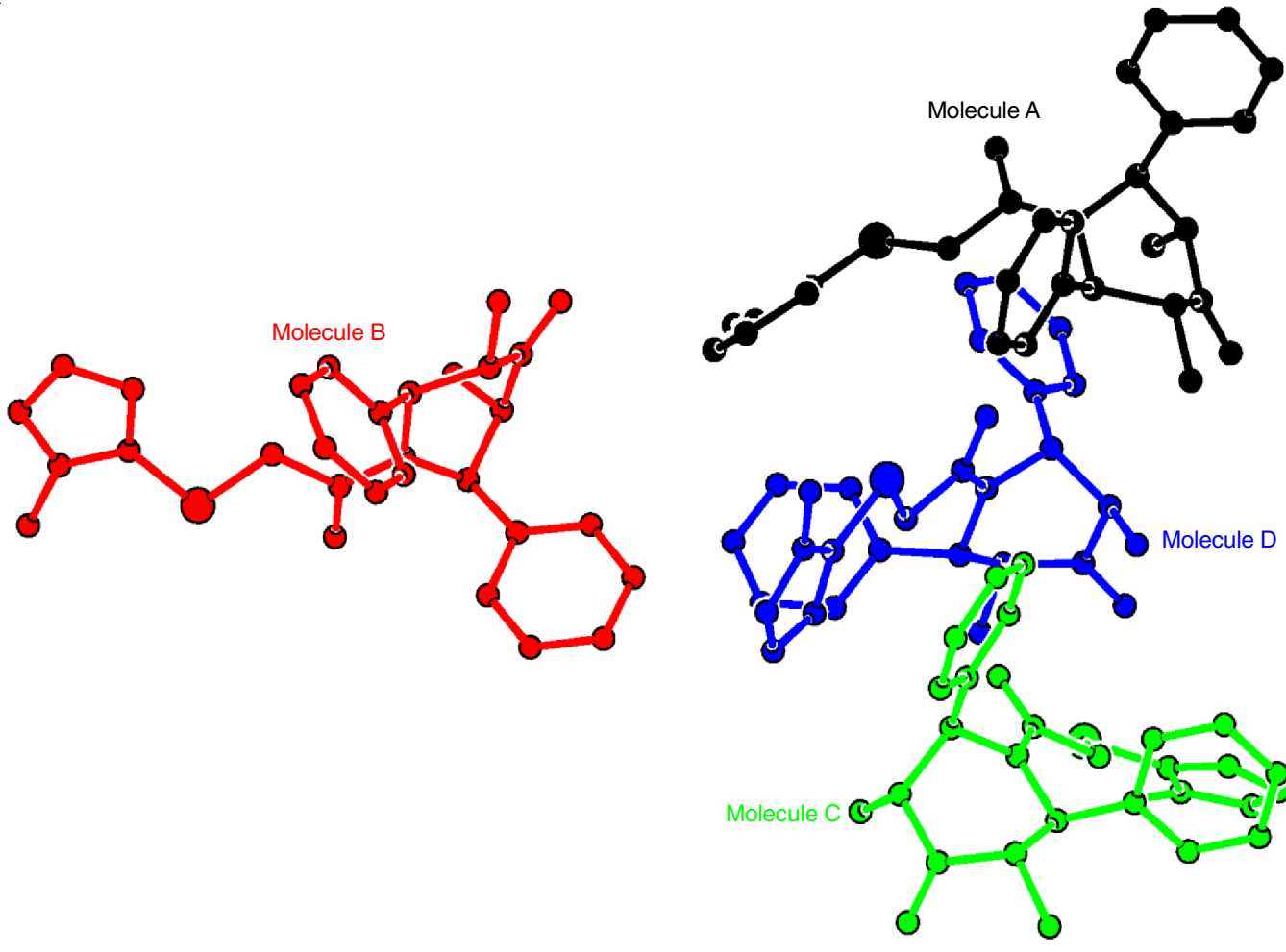


Fig. 5. Four molecules in the asymmetric unit of DMTSDPO

TABLE-3 BOND LENGTHS (Å) OF THE HYDROGEN ATOMS FOR DMTSDPO SINGLE CRYSTAL							
Molec	cule A	Mole	cule B	Molecule C		Molecule D	
Atoms	Length	Atoms	Length	Atoms	Length	Atoms	Length
C2-H2	0.98	C2-H2	0.98	C2-H2C	0.98	C2-H2	0.98
C3-H3	0.98	С3-Н3	0.98	С3-Н3С	0.98	C3-H3	0.98
C5-H5	0.98	C5-H5	0.98	C5-H5C	0.98	C5-H5	0.98
C6-H6	0.98	C6-H6	0.98	C6-H6C	0.98	C6-H6	0.98
C8-H8	0.93	C8-H8	0.93	C8-H8C	0.93	C8-H8	0.93
C9-H9	0.93	C9-H9	0.93	С9-Н9С	0.93	C9-H9	0.93
C10-H10	0.93	C10-H10	0.93	C10-H10	0.93	C10-H10	0.93
C11-H11	0.93	C11-H11	0.93	C11-H11	0.93	C11-H11	0.93
C12-H12	0.93	C12-H12	0.93	C12-H12	0.93	C12-H12	0.93
C14-H14	0.93	C14-H14	0.93	C14-H14	0.93	C14-H14	0.93
C15-H15	0.93	C15-H15	0.93	C15-H15	0.93	C15-H15	0.93
C16-H16	0.93	C16-H16	0.93	C16-H16	0.93	C16-H16	0.93
C17-H17	0.93	C17-H17	0.93	C17-H17	0.93	C17-H17	0.93
C18-H18	0.93	C18-H18	0.93	C18-H18	0.93	C18-H18	0.93
C19-H19A	0.96	C19-H19D	0.96	C19-H19G	0.96	C19–H19J	0.96
C19-H19B	0.96	C19-H19E	0.96	C19-H19H	0.96	C19-H19K	0.96
C19-H19C	0.96	C19-H19F	0.96	C19-H19I	0.96	C19-H19L	0.96
C20-H20A	0.96	C20-H20D	0.96	C20-H20G	0.96	C20-H20J	0.96
C20-H20B	0.96	C20-H20E	0.96	C20-H20H	0.96	C20-H20K	0.96
C20-H20C	0.96	C20-H20F	0.96	C20-H20I	0.96	C20-H20L	0.96
C22-H22A	0.97	C22-H22C	0.97	C22-H22E	0.97	C22-H22G	0.97
C22-H22B	0.97	C22-H22D	0.97	C22-H22F	0.97	C22-H22H	0.97
C24-H24A	0.96	C24-H24D	0.96	C24-H24G	0.96	C24-H24J	0.96
C24-H24B	0.96	C24-H24E	0.96	C24-H24H	0.96	C24-H24K	0.96
C24-H24C	0.96	C24-H24F	0.96	C24-H24I	0.96	C24-H24L	0.96

a confirmation supported by puckering [50] and asymmetry parameters [51]. Specifically, for molecule A, the distorted boat conformation parameters are as follows: $q^2 = 0.703$ (2) Å, $q^3 = -0.020$ (2) Å, $q^2 = 303.18$ (2)° and $q^2 = 0.020$ (2) Å, $q^2 = 303.18$ (2)° and $q^2 = 0.020$ (2)°.

The sulfanylacetyl group O1-C21-C22-S1 torsion angles, which connect the piperidine and tetrazole groups, exhibit variations across the four molecules: -0.7 (3)° for molecule A, -27.0 (2)° for molecule B, 26.9 (2)° for molecule C and -0.3 (4)° for molecule D. The S1-C21-C22-N1 torsion angles, involving the nitrogen N atoms, are 179.65(17)° for molecule A, 154.77(15)° for molecule B, 154.66 (15)° for molecule C and 179.69 (17)° for molecule D. All four molecules maintain their relative arrangement in the solid-state construction.

The distances of the carbonyl (C=O) group in the four molecules, approximately 1.212 (3) Å, are similar to 3-isopropyl-1-{2-[(1-methyl-1*H*-tetra-zol-5-yl)sulfan-yl]acet-yl}-2,6-diphenyl-piperidin-4-one hemihydrates [52]. The crystallographically independent molecules are similar in terms of carbonyl distances: 1.217 (3) Å for molecule A, 1.208 (3) Å for molecule B, 1.209 (3)Å for molecule C and 1.214 (3)Å for molecule D. In all four molecules, the carbonyl category is *anti*-oriented to C2 [C2–N1–C21–O2=] at -175.28(19)° and *syn*-oriented to C6 [C6–N1–C21–O2=] at -4.6(3)°.

For molecules A, B and C, the methyl atoms C19 & C20 are in equatorial and axial orientations, while in molecule D, this arrangement is opposite to the three other molecules (A, B & D), based on the torsion angle values for atom C19, N1\C2\C3\C19 [-178.85(19), 172.32(17), -171.98(17) & 67.5

(3)] and for atom C20 [68.0(3), -79.8(2), 80.0(2) & -178.78 (19)].

The dihedral angle between the connected phenylrings [C7–C12 and C13–C18] encloses the piperidine ring's most effective plane, with angles of 85.82(12) and 62.17(11)°. The two phenyl rings [C7–C12 and C13–C18] aligned to one another at a dihedral angle of 67.76(12)°, as demonstrated for molecule A. The tetrazole ring is plane, with an ultimate deviation of 0.002 (3)°. The tetrazole ring is planar in all four molecules, with the maximum deviation observed for the N4 atom. In all four molecules, the endocyclic bond lengths of N2–N3 (1.368 (3)°, 1.353 (3), 1.350(3) & 1.375(3)), N3–N4 (1.279 (4) Å, 1.274(4), 1.277 (4) & 1.282(4)) and N4–N5 (1.343 (4) Å, 1.344(3), 1.349(3), & 1.344(4)) indicate alternate single and double bonds.

Packing features: The crystalline stuffing of the molecules is intricately connected *via* a network of C–H···O and C–H···N intra- and intermolecular connections. All four molecules exhibit robust C–H···O intra- and intermolecular connections, forming distinct hydrogen bond graph-set motifs. Molecules B and C are interconnected through C–H···O and C–H···N hydrogen bonds. The C–H···N and C–H···O hydrogen bonds contribute to the formation of a dimer with an R22(10) ring motif. Additionally, an intramolecular C–H···O hydrogen bond completes a chain, resulting in an S(7) motif [53], as depicted in Fig. 6. Paired C–H···O hydrogen bonds further link the molecules into centrosymmetric R22(14) dimers, as illustrated in Fig. 7. The details of hydrogen bonding and non-bonded interactions for DMTSDPO [Å and °] are provided in Table-4.

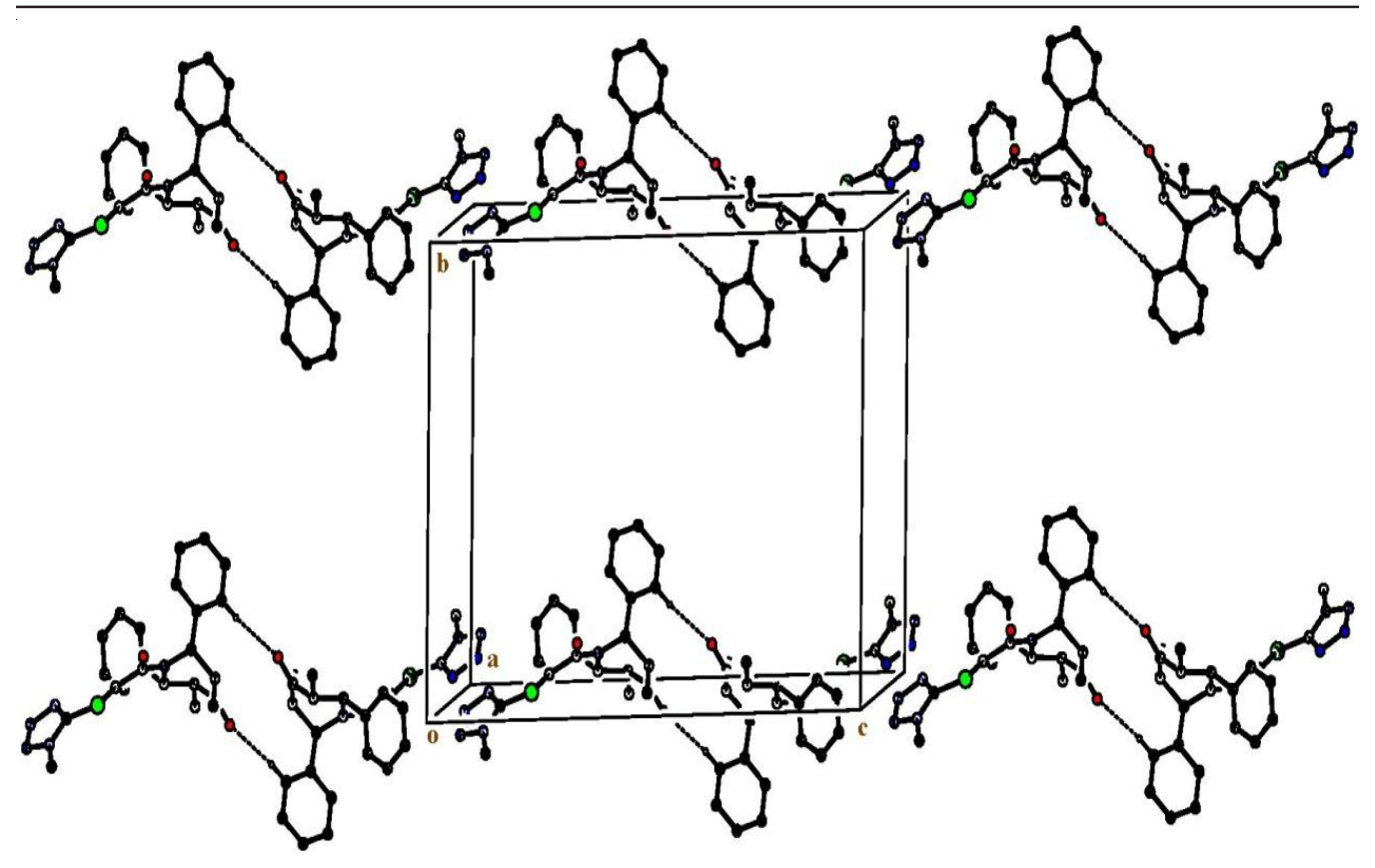


Fig. 6. C–H···N and C–H···O hydrogen bonds establishing a dimer of $R_2^2(10)$ ring modification

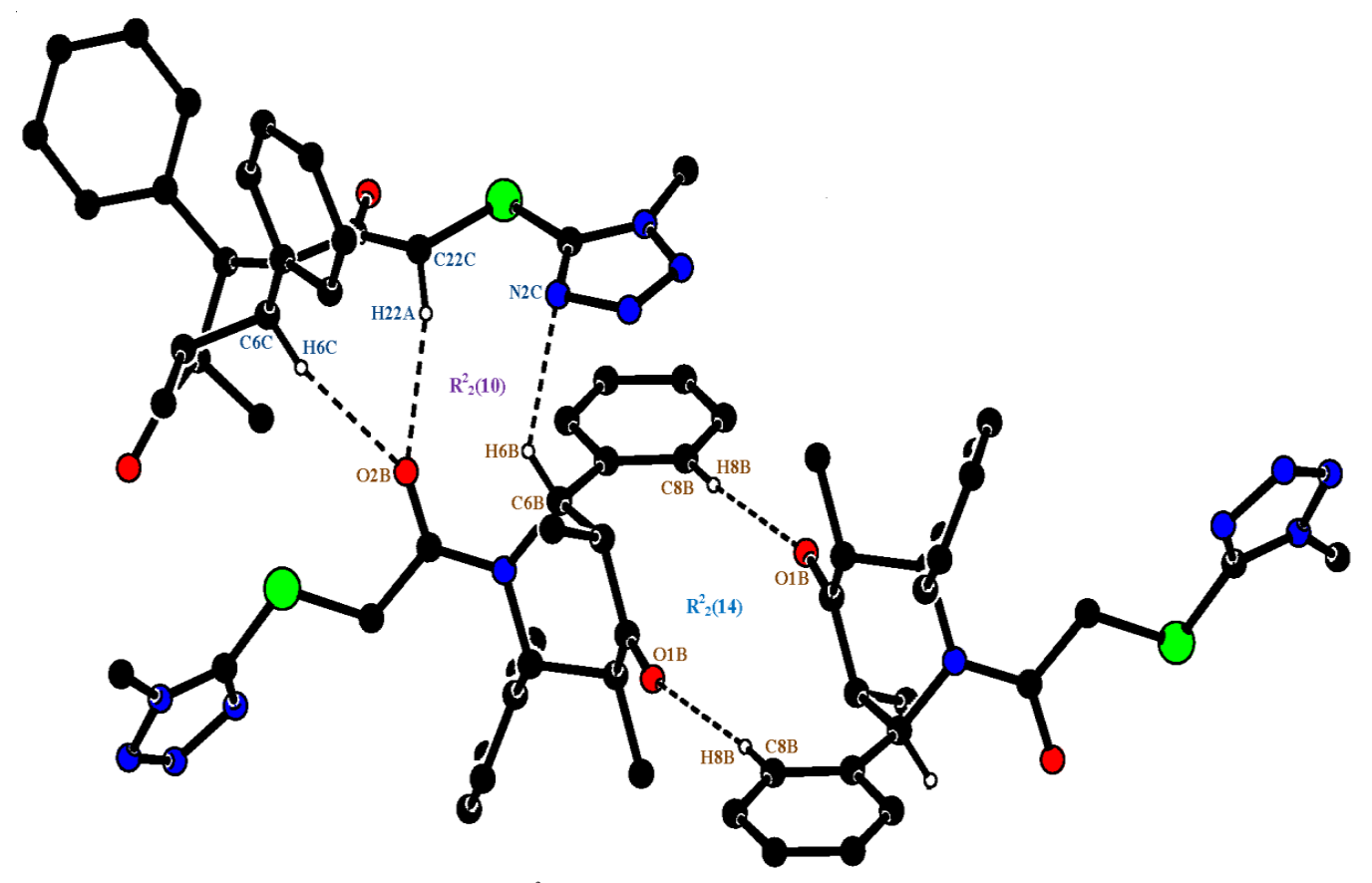


Fig. 7. C-H···O interaction forming a R₂(10) dimer as shown packed mode of molecules observed down a-axis

TABLE-4 HYDROGEN BONDING AND NON-BONDED INTERACTIONS FOR DMTSDPO [Å AND °]					
D–H···A	d(D-H)	$d(H \cdot \cdot \cdot A)$	$d(D \cdot \cdot \cdot A)$	∠(DHA)	
C6-H6···O2C	0.98	2.47	3.405(3)	160	
C6A-H6A···O2	0.98	2.40	3.359(2)	167	
C22-H22B···O2C	0.97	2.37	3.302(3)	160	
C22A-H22C···O2	0.97	2.30	3.186(3)	151	
C2A-H2A···N2Bi	0.98	2.57	3.331(3)	134	
C6B-H6B···O2Ai	0.98	2.46	3.397(3)	160	
C6C-H6C···O2B ⁱⁱ	0.98	2.40	3.363(3)	167	
C18A–H18A···O1A ⁱⁱⁱ	0.93	2.51	3.434(3)	172	
C18C-H18C···O1C ^{iv}	0.93	2.52	3.443(3)	171	
C22B-H22E···O2Ai	0.97	2.38	3.303(3)	159	
C22C-H22H···O2B ⁱⁱ	0.97	2.30	3.190(3)	152	

Equivalent position code:

i = -x,1-y,1-z ii = 1-x,-y,1-z iii = 1-x,1-y,-ziv = 2-x,-y,1-z

Hirshfeld surface analysis: In Fig. 8, the hydrogen bond surface (HS) plotted over the density norm (d_{norm}) reveals that the white surface region corresponds to contacts by distances equally to total number of van der Waals radii. A shorter distance

is represented in close contacts (red colour), while a longer distance indicates distinct contacts (blue colour) associated to the total number of van der Waals radii, respectively [54]. Fig. 9a-l illustrates the overall 2D fingerprint plot and specific categories, including H···H/H···H, H···N/N···H, C···H/H···C, H···O/ $O\cdots H$, $H\cdots S/S\cdots H$, $N\cdots O/O\cdots N$, $N\cdots S/S\cdots N$, $C\cdots C/C\cdots C$, $C\cdots N/O\cdots N$ N···C, C···O/O···C, C···S/S···C & O···S/S···O contacts. The predominant interaction is H···H, contributing 54.8% to the complete crystal packing (Fig. 9a). The 2D fingerprint plot reveals a pair of spikes delineated into H···N/N···H contacts with an 18.7% involvement to the hydrogen bond surface (HS) (Fig. 9b), showing a symmetric distribution of points. The remaining contributions, representing hydrogen bonds C···H/H···C, H···O/ $O\cdots H$, $H\cdots S/S\cdots H$, $N\cdots O/O\cdots N$, $N\cdots S/S\cdots N$, $C\cdots C/C\cdots C$, $C\cdots N/O\cdots N$ N···C, C···O/O···C, C···S/S···C & O···S/S···O contacts, are detailed in Fig. 9c–l, respectively.

Molecular docking studies of piperidine derivatives with DPP4 as a target protein: Dipeptidyl peptidase IV (DPP4) [55] is a key enzyme in the anti-diabetic pathway. Inhibitors of DPP4 are currently being developed as an emerging category of therapeutic medicines for the treatment of diabetes, either by themselves or combined with other anti-diabetic medications. DPP4 protein molecules, which include SYR-322 and

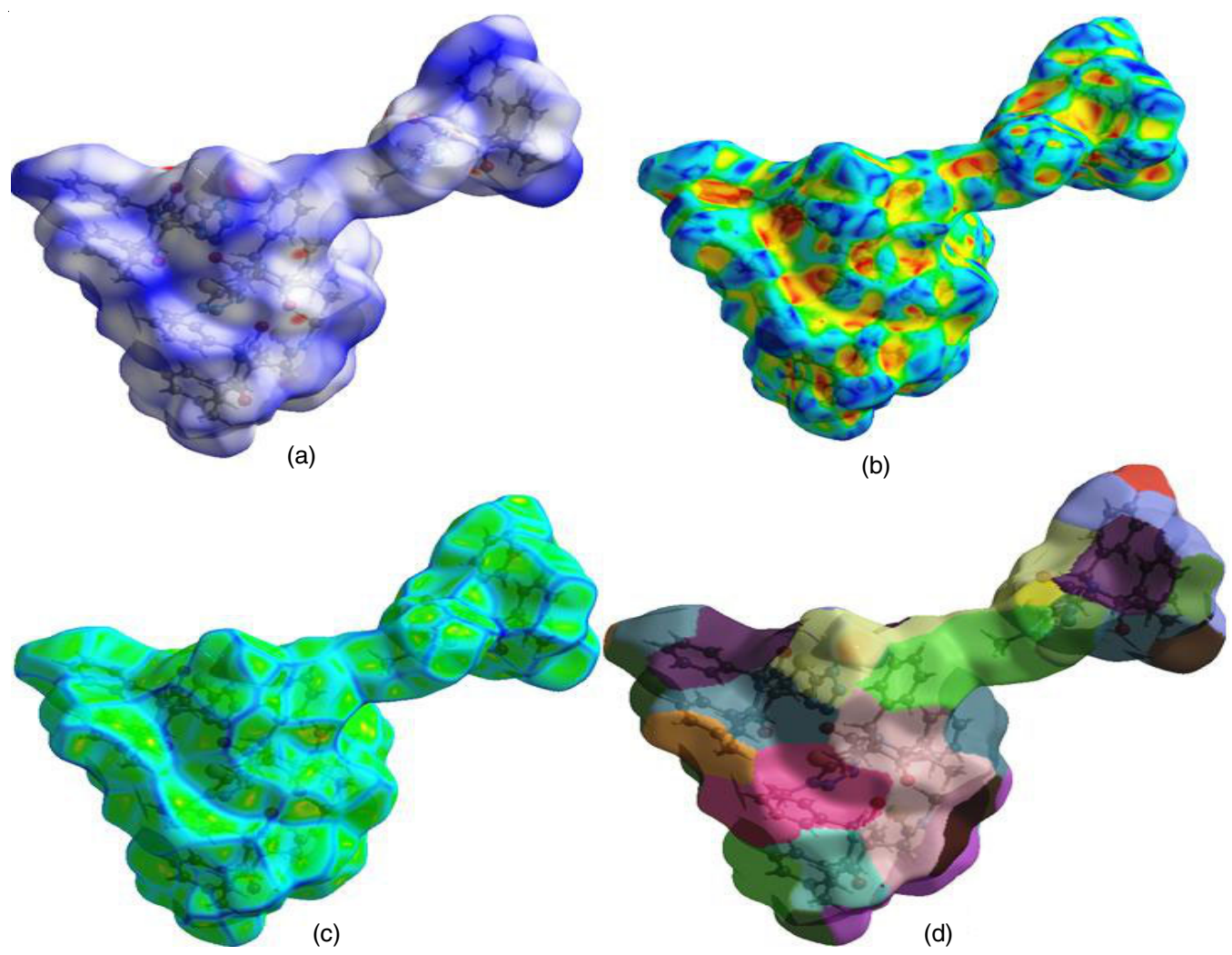


Fig. 8. Hirshfeld surface evaluation of DMTSDPO mapped over d_{norm}, showing the close contacts

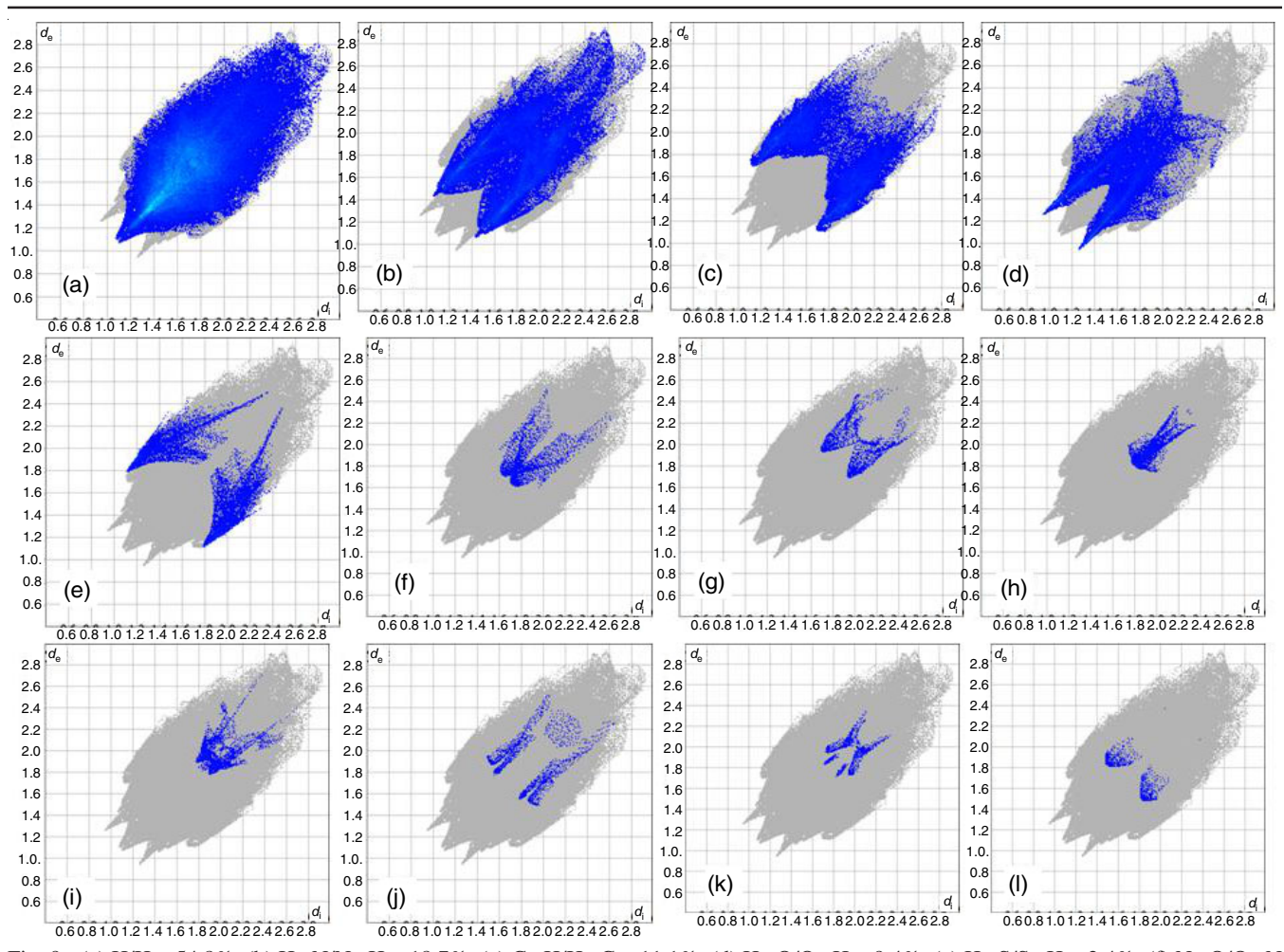


Fig. 9. (a) H/H = 54.8%; (b) H···N/N···H = 18.7%; (c) C···H/H···C = 11.1%; (d) H···O/O···H = 9.4%; (e) H···S/S···H = 2.4%; (f) N···O/O···N = 0.7%; (g) N···S/S···N = 0.7%; (h) C···C/C···C = 0.6%; (i) C···N/N···C = 0.6%; (j) C···O/O···C = 0.5%; (k) C···S/S···C = 0.3%; (l) O···S/S···O = 0.2%

ABT-279, are either eagerly awaiting regulatory approval or in human clinical research. Piperidine derivatives bind effectively to DPP4's active site pocket and interact with its amino acid residues, according to molecular docking studies.

The title compound DMTSDPO is an effective inhibitor, as shown in Fig. 10. Nitrogen and oxygen atoms in DMTSDPO form strong connections with Ser630 and Arg125 at distances of 3.13 Å and 3.40 Å, respectively. Furthermore, the co-crystal ligand docks effectively in active site region of the embattled protein, demonstrating interactions commonly observed when DMTSDPO binds at the active site. A depiction of the molecule DMTSDPO in DDP4 active site showcases the crucial hydrogen contacts with the piperidine derivatives and enzyme, as presented in Fig. 11. Table-5 provides information on hydrogen bond interactions, docking scores and binding energy of DMT-SDPO molecule and the co-crystal ligand with DPP4 receptor.

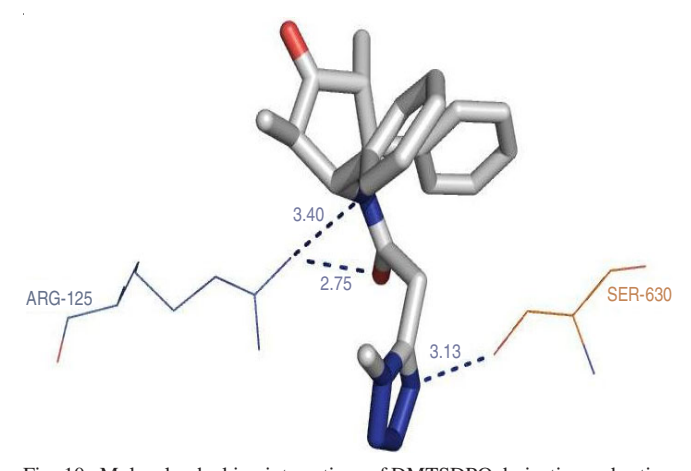


Fig. 10. Molecular docking interactions of DMTSDPO derivative and active site residues

TABLE-5 HYDROGEN BOND INTERACTIONS OF DMTSDPO AND CO-CRYSTAL LIGAND WITH DPP4 RECEPTOR					
Ligand	Glide score	Glide energy (kcal/mol)	Interaction	Distance (Å)	
Co-crystal	-3.967	-31.133			
DMTSDPO	-5.071	-38.570	ARG125 [N···H–N]	3.40	
			ARG125 [N–H···O]	2.75	
			SER630 [O-HN]	3.13	

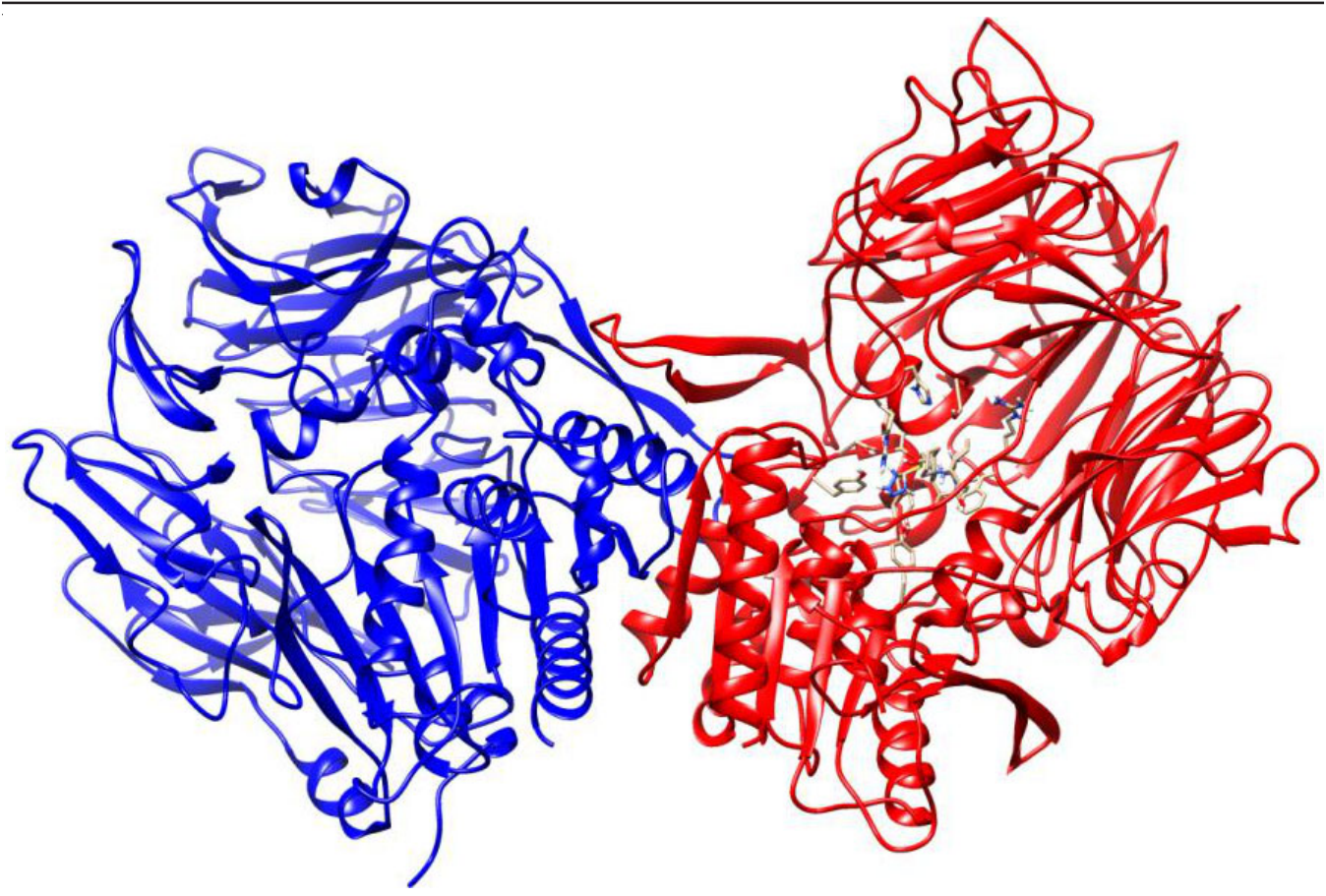


Fig. 11. A perspective towards the DMTSDPO molecule in the DDP4 active site

Conclusion

Single crystal of 3,5-dimethyl-1-[2-(1-methyltetrazol-5yl)sulfanylacetyl]-2,6-diphenyl-piperidin-4-one (DMTSDPO) has demonstrated successful with detail investigations and analyzed using X-ray diffraction methods. Hirshfeld surface evaluation and 2D finger plots have been employed to observe better intermolecular and intramolecular interactions in the crystal packing system of DMTSDPO molecule. Hirshfeld surface evaluation reveals that H···H/H···H and C···H/H···C are the most abundant intermolecular interactions. This evidence is valuable for understanding the role of van der Waals forces in influencing the stabilization of molecular packing. Moreover, piperidine derivatives have been subjected to molecular docking with the targeted protein dipeptidyl peptidase IV (DPP4), a crucial enzyme in the anti-diabetic pathway. The observed docking scores and hydrogen bond interactions are discussed, providing insights into the potential mechanisms of action for these compounds. The DMTSDPO compound demonstrates effective antimicrobial operations towards Gram-positive organisms, specifically S. aureus and S. pyogenes, with ampicillin used as drug standard.

CONFLICT OF INTEREST

The authors declare that there is no conflict of interests regarding the publication of this article.

REFERENCES

- H.I. El-Subbagh, S.M. Abu-Zaid, M.A. Mahran, F.A. Badria and A.M. Al-Obaid, *J. Med. Chem.*, 43, 2915 (2000); https://doi.org/10.1021/jm000038m
- M.V. Muppuli, K. Rajesh, D. Anitha Rexalin, K. Anandan, K. Gayathri, A. Mani, P. Devendran, V. Thayanithi, P. Kurinjinathan and M. Suresh Kumar, J. Struct. Chem., 65, 987 (2024); https://doi.org/10.1134/S0022476624050123
- R.V. Perumal, M. Adiraj and P. Shanmugapandiyan, *Indian Drugs*, 38, 156 (2001).
- M. Hoffelner, W. Seebacher, U. Hassan, A. Leitner, R. Weis and R. Saf, *Tetrahedron*, 90, 132189 (2021); https://doi.org/10.1016/j.tet.2021.132189
- S.K. Sahu, B.K. Dubey, A.C. Tripathi, M. Koshy and S.K. Saraf, *Mini Rev. Med. Chem.*, 13, 565 (2013);
- https://doi.org/10.2174/1389557511313040009

 6. A.R. Katritzky and W. Fan, *J. Org. Chem.*, **55**, 3205 (1990); https://doi.org/10.1021/jo00297a041
- C.R. Ganellin and R.G.W. Spickett, *J. Med. Chem.*, 8, 619 (1965); https://doi.org/10.1021/jm00329a015
- A.M. Priya, M. Manikandan, G. Kalaiselvi, P. Arun, P. Chinnaswamy and K. Selvam, *Asian J. Microbiol. Biotechnol. Environ. Sci.*, 9, 1049 (2007).
- 9. I.E. Bylov, M.V. Vasylyev and Y.V. Bilokin, Eur. J. Med. Chem., 34, 997 (1999);
 - https://doi.org/10.1016/S0223-5234(99)00119-1
- C. Dollery, Therapeutic Drugs, Churchill Livingstone, Edinburgh, Vol. I, edn. 3 (1999).
- 11. O.P. Robinson, Postgrad. Med. J., 49(Suppl 4), 9 (1973).
- S. Bashwira and C. Hootele, *Tetrahedron*, 44, 4521 (1988); https://doi.org/10.1016/S0040-4020(01)86153-6

- R. Ramachandran, P. Parthiban, A. Doddi, V. Ramkumar and S. Kabilan, *Acta Cryst. E*, 63, o4559 (2007); https://doi.org/10.1107/S1600536807054165
- S. Balamurugan, A. Thiruvalluvar, R.J. Butcher, A. Manimekalai and J. Jayabharathi, *Acta Cryst. E*, 64, o59 (2008); https://doi.org/10.1107/S1600536807062204
- A. Thiruvalluvar, S. Balamurugan, R.J. Butcher, A. Manimekalai and J. Jayabharathi, *Acta Cryst. E*, 63, o4533 (2007); https://doi.org/10.1107/S1600536807053846
- D. Gayathri, D. Velmurugan, R.R. Kumar, S. Perumal and K. Ravikumar, *Acta Cryst. E*, 64, o520 (2008); https://doi.org/10.1107/S1600536808002286
- D.A. Winkler and G. Holan, J. Med. Chem., 32, 2084 (1989); https://doi.org/10.1021/jm00129a011
- M. Elena, J.M. Quero, C.L. Tarrida and L.G. Franquelo, Design of a Mobile Telecardiology System using GPRS/GSM Technology, Proceedings of the Second Joint 24th Annual Conference and the Annual Fall Meeting of the Biomedical Engineering Society, Houston, TX, USA, vol. 3, pp. 1859-1860 (2002);
- https://doi.org/10.1109/IEMBS.2002.1053063
- B.A. Wexler, B.H. Toder, G. Minaskanian and A.B. Smith III, *J. Org. Chem.*, 47, 3333 (1982); https://doi.org/10.1021/jo00138a030
- M.A. Vasquez, E. Iniguez, U. Das, S.M. Beverley, L.J. Herrera, J.R. Dimmock and R.A. Maldonado, *Antimicrob. Agents Chemother.*, 59, 3598 (2015); https://doi.org/10.1128/AAC.04056-14
- B. Mutus, J.D. Wagner, C.J. Talpas, J.R. Dimmock, O.A. Phillips and R.S. Reid, *Anal. Biochem.*, 177, 237 (1989); https://doi.org/10.1016/0003-2697(89)90045-6
- C.R. Noller and V. Baliah, J. Am. Chem. Soc., 70, 3853 (1948); https://doi.org/10.1021/ja01191a092
- G.V. Grishina, E.L. Gaidarova and N.S. Zefirov, *Chem. Heterocycl. Compd.*, 30, 1401 (1995); https://doi.org/10.1007/BF01172866
- R. Jeyaraman, S. Ponnuswamy, M. Venkatraj, M. Sureshkumar, D. Kumaran and M.N. Ponnuswamy, *Indian J. Chem.*, 41B, 614 (2002).
- M. Nalanishi, M. Shiraki, T. Kobayakawa and R. Kobayashi, (1974).
 Jpn Patent No. 74-03987.
- R. Badorrey, C. Cativiela, M.D. Díaz-de-Villegas and J. Gálvez, *Tetrahedron*, 55, 7601 (1999); https://doi.org/10.1016/S0040-4020(99)00377-4
- G. Aridoss, S. Balasubramanian, P. Parthiban, R. Ramachandran and S. Kabilan, *Med. Chem. Res.*, 16, 188 (2007); https://doi.org/10.1007/s00044-007-9023-x
- G. Aridoss, S. Balasubramanian, P. Parthiban and S. Kabilan, *Eur. J. Med. Chem.*, 42, 851 (2007); https://doi.org/10.1016/j.ejmech.2006.12.005
- G. Aridoss, P. Parthiban, R. Ramachandran, M. Prakash, S. Kabilan and Y.T. Jeong, Eur. J. Med. Chem., 44, 577 (2009); https://doi.org/10.1016/j.ejmech.2008.03.031
- G. Aridoss, S. Amirthaganesan, M.S. Kim, B.G. Cho, K.T. Lim and Y.T. Jeong, *ARKIVOC*, 133 (2008); https://doi.org/10.3998/ark.5550190.0009.f14
- G. Aridoss, D. Gayathri, D. Velmurugan, M.S. Kim and Y.T. Jeong, *Acta Cryst. E*, 65, o1708 (2009); https://doi.org/10.1107/S1600536809023836
- A. Palani, S. Shapiro, H. Josien, T. Bara, J.W. Clader, J.M. Strizki, K. Cox, W.J. Greenlee and B.M. Baroudy, *J. Med. Chem.*, 45, 3143 (2002); https://doi.org/10.1021/jm0200815
- P.M. Weintraub, J.S. Sabol, J.M. Kane and D.R. Borcherding, *Tetrahedron*, 59, 2953 (2003); https://doi.org/10.1016/S0040-4020(03)00295-3

- R.V. Perumal, M. Adiraj and P. Shanmuga Pandiyan, *Indian Drugs*, 38, 156 (2001).
- 35. C. Ramalingan, Y.T. Park and S. Kabilan, *Eur. J. Med. Chem.*, **41**, 683 (2006);
 - https://doi.org/10.1016/j.ejmech.2006.02.005
- S. Balasubramanian, G. Aridoss, P. Parthiban, C. Ramalingan and S. Kabilan, *Biol. Pharm. Bull.*, 29, 125 (2006); https://doi.org/10.1248/bpb.29.125
- M. Srinivasan, S. Perumal and S. Selvaraj, *Chem. Pharm. Bull.*, 54, 795 (2006); https://doi.org/10.1248/cpb.54.795
- Bruker, APEX2, SAINT. Bruker AXS Inc. Madison Wisconsin, USA (2004).
- G.M. Sheldrick, SADABS, Software for Empirical Absorption Corrections, University of Göttingen, Göttingen (1996).
- G.M. Sheldrick, Acta Crystallogr. A, 64, 112 (2008); https://doi.org/10.1107/S0108767307043930
- 41. A.L. Spek, *Acta Cryst. D*, **65**, 148 (2009); https://doi.org/10.1107/S090744490804362X
- L.J. Farrugia, J. Appl. Cryst., 30, 565 (1997); https://doi.org/10.1107/S0021889897003117
- M.J. Turner, J.J. McKinnon, S.K. Wolff, D.J. Grimwood, P.R. Spackman, D. Jayatilaka and M.A. Spackman, CrystalExplorer17, University of Western Australia (2017).
- J.J. McKinnon, D. Jayatilaka and M.A. Spackman, *Chem. Commun.*, 3814 (2007); https://doi.org/10.1039/b704980c
- P.R. Spackman, M.J. Turner, J.J. McKinnon, S.K. Wolff, D.J. Grimwood,
 D. Jayatilaka and M.A. Spackman, J. Appl. Cryst., 54, 1006 (2021);
 https://doi.org/10.1107/S1600576721002910
- Z. Pei, X. Li, T.W. von Geldern, K. Longenecker, D. Pireh, K.D. Stewart, B.J. Backes, C. Lai, T.H. Lubben, S.J. Ballaron, D.W.A. Beno, A.J. Kempf-Grote, H.L. Sham and J.M. Trevillyan, *J. Med. Chem.*, 50, 1983 (2007); https://doi.org/10.1021/jm061436d
- R.A. Friesner, J.L. Banks, R.B. Murphy, T.A. Halgren, J.J. Klicic, D.T. Mainz, M.P. Repasky, E.H. Knoll, M. Shelley, J.K. Perry, D.E. Shaw, P. Francis and P.S. Shenkin, *J. Med. Chem.*, 47, 1739 (2004); https://doi.org/10.1021/jm0306430
- P.A. Wayne National Committee for Clinical Laboratory Standards. Performance Standards for Antimicrobial Disc Susceptibility Testing, edn. 12, CLSI standard M02. Wayne, PA: Clinical and Laboratory Standards. Institute (2002).
- N.B. Patel and J.C. Patel, Sci. Pharm., 78, 171 (2010); https://doi.org/10.3797/scipharm.0912-16
- N.K. Fuloria, V. Singh, M. Shaharyar and M. Ali, *Molecules*, 14, 1898 (2009); https://doi.org/10.3390/molecules14051898
- D.T. Cremer and J.A. Pople, J. Am. Chem. Soc., 97, 1354 (1975); https://doi.org/10.1021/ja00839a011
- M. Nardelli, Acta Crystallogr. C, 39, 1141 (1983); https://doi.org/10.1107/S0108270183007696
- S. Ganesan, P. Sugumar, S. Ananthan and M.N. Ponnuswamy, *Acta Cryst. E*, 69, o1598 (2013); https://doi.org/10.1107/S1600536813026500
- J. Bernstein, R.E. Davis, L. Shimoni and N.L. Chang, *Angew. Chem. Int. Ed. Engl.*, 34, 1555 (1995); https://doi.org/10.1002/anie.199515551
- P. Venkatesan, S. Thamotharan, A. Ilangovan, H. Liang and T. Sundius, *Spectrochim. Acta A Mol. Biomol. Spectrosc.*, 153, 625 (2016); https://doi.org/10.1016/j.saa.2015.09.002